

Published in final edited form as:

J Neurosci. 2012 May 9; 32(19): 6688–6698. doi:10.1523/JNEUROSCI.0081-12.2012.

Dynamic changes in interneuron morpho-physiological properties mark the maturation of hippocampal network activity

C. Allene^{1,2,3}, M. A. Picardo^{1,2,3}, H. Becq^{1,2,3}, G. Miyoshi⁴, G. Fishell⁴, and R. Cossart^{1,2,3,*}

¹Inserm Unité 901, Marseille, 13009, France

²Université de la Méditerranée, UMR S901 Aix-Marseille 2, 13009, France

³INMED, Marseille 13009, France

⁴NYU Neuroscience Institute and the Depts of Physiology and Neuroscience, and Neural Science. NYU Langone Medical Center, 522, 1st Ave. NY, NY, 10016, USA

Abstract

During early postnatal development, neuronal networks successively produce various forms of spontaneous patterned activity that provide key signals for circuit maturation. Initially, in both rodent hippocampus and neocortex, coordinated activity emerges in the form of Synchronous Plateau Assemblies (SPAs) that are initiated by sparse groups of gap-junction coupled oscillating neurons. Subsequently, SPAs are replaced by synapse-driven Giant Depolarizing Potentials (GDPs). Whether these sequential changes in mechanistically distinct network activities correlate with modifications in single-cell properties is unknown. To understand this, we have studied the morpho-physiological fate of single SPA-cells as a function of development. We focused on CA3 GABAergic interneurons, which are centrally involved in generating GDPs in the hippocampus. As the network matures, GABAergic neurons are engaged more in GDPs and less in SPAs. Using inducible genetic fate mapping, we show that the individual involvement of GABAergic neurons in SPAs is correlated to their temporal origin. In addition, we demonstrate that the SPA to GDP transition is paralleled by a remarkable maturation in the morpho-physiological properties of GABAergic neurons. Compared to those involved in GDPs, interneurons participating in SPAs possess immature intrinsic properties, receive synaptic inputs spanning a wide amplitude range, and display large somata as well as membrane protrusions. Thus, a developmental switch in the morpho-physiological properties of GABAergic interneurons as they progress from SPA to GDPs marks the emergence of synapse-driven network oscillations.

Introduction

As development proceeds, the changing dynamics of spontaneous coordinated neuronal activity is controlled by distinct cellular mechanisms, resulting in a stereotypic sequence being associated with the maturation of network activity patterns (Allene and Cossart, 2010; Blankenship and Feller, 2010). Interestingly, the timing and mechanisms utilized in the maturation of spontaneous patterned activity is remarkably robust across brain structures, indicating that the signals linking activity to the maturation of neurons and circuits could be widely conserved.

Still, it remains unknown whether the developmental sequences in network activity patterns impact the morpho-physiological properties of the individual neurons. Addressing this issue is crucial for understanding the role of activity in development, as it should help elucidate

*To whom correspondence should be addressed. cossart@inmed.univ-mrs.fr.

the influence of early correlated activities on the maturation of specific single-cell properties.

We have recently dissected the maturation of correlated activity patterns in both the rodent hippocampus and neocortex using electrophysiology and calcium imaging (Allene et al., 2008; Crepel et al., 2007). In both regions, the earliest coherent electrical patterns of activity emerge around birth in the form of Synchronous Plateau Assemblies (SPAs), so called because of their characteristic spatial-temporal dynamics: SPAs involve discrete groups of gap-junction-coupled neurons producing correlated calcium plateaus associated with suprathreshold membrane potential oscillations. SPAs are gradually switched off towards the end of the first postnatal week in rodents, when they are replaced by synapse-driven Giant Depolarizing Potentials (GDPs) (Ben Ari et al., 1989) that synchronize larger neuronal populations. Here we asked whether the involvement of an individual neuron in SPAs or GDPs is mirrored by changes in their specific morpho-physiological properties. We focused on GABAergic neurons for two reasons. First, GABAergic transmission is central for the generation of GDPs (Ben Ari et al., 1989; Bonifazi et al., 2009; Garaschuk et al., 1998; Sipila et al., 2005), suggesting that SPAs, by occurring before the onset of GDPs, could be a central step for the maturation of interneurons. Second, the GABAergic neuron population is characterized by its morpho-physiological diversity. If diverse subtypes are affected by early network activities in a similar way, it would imply that the impact of correlated activity is universal and cell type-independent.

Here we study the morpho-physiological changes in GABAergic interneurons at the transition period between SPA- and GDP- dominated networks in the CA3 region of the mouse hippocampus. We use a compound approach that combines chronic daily multineuron calcium imaging, targeted current- and voltage-clamp recordings, inducible genetic fate mapping and morphological analysis. We show that various types of GABAergic neurons are involved in SPAs and that the transition to a GDP activity pattern occurs during the first postnatal week. We demonstrate that the time when this transition occurs is correlated to the temporal embryonic origin of individual interneurons. Moreover, SPA-interneurons switch their morpho-physiological properties coincident with them receiving GDPs. The physiological diversity that characterizes the GABAergic neuron population only emerges once the SPA to GDP transition is completed. Taken together, these results show that the SPA to GDP network sequence is reflected at the single-cell level in the morpho-physiological evolution of GABAergic neurons.

Materials and Methods

Acute slice preparation and calcium imaging

All animal use protocols were performed under the guidelines of the French National Ethic Committee for Sciences and Health report on “Ethical Principles for Animal Experimentations” in agreement with the European Community Directive 86/609/EEC. Horizontal hippocampal slices (380 μ m thick) were prepared from 1 to 7-day-old (P1–7) GAD-67-GFP-KI mice (Tamamaki et al., 2003) or tamoxifen-treated *Mash1^{CreERTM};RCE:LoxP* mice (Miyoshi et al., 2010) using a vibratome (Leica Microsystems, microtomes VT1200 S) in ice-cold oxygenated modified artificial CSF (mACSF: 0.5 mM CaCl₂ and 7 mM MgSO₄; NaCl replaced by an equimolar concentration of choline). Slices were then transferred and allowed to recover (around 1 h) in oxygenated normal ACSF containing (in mM): 126 NaCl, 3.5 KCl, 1.2 NaH₂PO₄, 26 NaHCO₃, 1.3 MgCl₂, 2.0 CaCl₂, and 10 D-glucose, pH 7.4. For AM-loading, slices were incubated in 2.5 ml of oxygenated ACSF with 25 μ l of a 1 mM fura-2 AM solution (Molecular Probes; in 100% DMSO) for 20–30 min. Slices were incubated in the dark, and the incubation solution was maintained at 35°–37°C. During imaging, slices were perfused at a rate of 4 ml/min

with continuously aerated (95% O₂/5% CO₂) normal ACSF at 35–37°C. Imaging was performed with a multibeam two-photon laser scanning system (Triscope-LaVision Biotec) coupled to an Olympus microscope as previously described (Crepel et al., 2007). Images were acquired through a CCD camera (La Vision Imager 3QE), which typically resulted in temporal resolution of around 100 ms (2 × 2 binning, pixel size: 600 nm). Slices were imaged using a low-magnification, high-numerical-aperture objective (20x, NA 0.95, Olympus). The size of the imaged field was typically 430 × 380 μm². Imaging depth was focused on average 80 μm below the surface (range: 50–100 μm).

Organotypic slice culture preparation and calcium imaging

Organotypic slices were, with minor changes, prepared from the hippocampus of P3 GAD-67-GFP-KI mice according to a previously described procedure (Stoppini et al., 1991). Mice were decapitated after anesthesia and put on ice. Following the removal of the brain, hippocampal sections, 400 μm thick, were prepared using a tissue chopper (Mc Ilwain, U.S.A.) and collected in a PBS solution supplemented with 0.5% D-glucose. Slices were then placed onto Millicell-CM culture inserts (0.4 μm; Millipore). The inserts were placed into 35 mm culture dishes with 1 ml of medium: MEM (sigma) supplemented with 750 μl hepes 1 M, insulin 0.1 mg/L (solution 5 mgr/ml 50X) and horse serum (20%, Gibco) at pH 7.25–7.29. Slices were maintained in a cell culture incubator at 37°C, in an atmosphere containing 5% CO₂. Imaging was performed on the second and third day following slice preparation. Slices were left in their initial culture plates with the MEM for the entire experimental protocol. For AM-loading, 1 ml of regular, but filtered, slice-ACSF as well as 2 μl of a 1 mM Fura-2AM solution (Molecular Probes; in 100% DMSO) were added for 20–30 min in the cell culture incubator. Just before calcium imaging, 1 ml of freshly filtered ACSF was added onto the slices and removed just after. For pharmacological experiments, 1 ml of filtered ACSF containing 10 μM of bumetanide (Sigma) was added onto the slice. The culture plate was kept in the cell culture incubator for 15 minutes prior to the imaging session. Each culture plate that contained slices to be chronically imaged, was manipulated under a sterile atmosphere to avoid culture contamination. Also the microscope objective was sterilized prior to each imaging session.

Analysis

As previously described (Crepel et al., 2007), analysis of the calcium activity was performed with custom-made software written in Matlab (MathWorks). This program aimed at the automatic identification of loaded cells and at measuring their fluorescence as a function of time. The calcium signal from each cell was determined as the average fluorescence within the contour of that cell, measured as a function of time. MiniAnalysis software (Synaptosoft) signal-processing algorithms were used to detect the onsets and offsets (time of half-amplitude decay) of calcium signals within the traces of individual cells. Active cells were considered to be neurons exhibiting at least one calcium event within the period of recording. The frequency of a network pattern was the averaged time interval between two peaks of synchronous activity. The incidence was the fraction of slices in which it could be recorded at least once. The amplitude of a network pattern in a given movie was the average of the maximum number of cells coactive in each peak of synchrony across the movie. To identify peaks of synchronous activity that included more cells than expected by chance, we used interval reshuffling (randomly reordering of intervals between events for each cell) to create a set of surrogate event sequences. Reshuffling was performed 1000 times for each movie, and a surrogate histogram was constructed for each reshuffling. The threshold corresponding to a significance level of $p < 0.05$ was estimated as the number of coactive cells exceeded in a single frame in only 5% of these histograms. The entire procedure could be performed on-line sufficiently quickly to identify cells for targeted patch-clamp recordings.

For the analysis of organotypic slice experiments, the difficulty was to track the position of single-cells across days as the soma location of neurons tends to move mostly due to the continuous slice flattening that occurs in the culture plate. Typically, focal planes from three different depths are necessary to recover all the cells imaged within a one-day interval. Easily recognizable visual cues provided by the GFP labelling were used to ensure that imaging was always from the same set of neurons.

Electrophysiology

Neurons were patch-clamp recorded in the whole-cell configuration. Microelectrode resistance was 4–8 M Ω . Uncompensated access resistance was monitored throughout the recordings. Values <20 M Ω were considered acceptable and the results were discarded if it changed by >20%. Whole-cell measurements were filtered at 3 kHz using a patch-clamp amplifier (HEKA, EPC10). Recordings were digitized on-line (20 kHz) with a Labmaster interface card to a personal computer and acquired using Axoscope 7.0 software (Molecular Devices). Synchronization between optical and electrical signals was achieved by feeding simultaneously the Labmaster interface card with the trigger signals for each movie frame and the electrophysiological recordings. For voltage-clamp experiments, the composition of the intracellular solution was: 120 mM Cs-gluconate, 10 mM MgCl₂, 0.1 mM CaCl₂, 1 mM EGTA, 5 mM Na₂ adenosine triphosphate, 10 mM HEPES. With this solution, glutamate-R-mediated postsynaptic currents (PSCs) reversed at +10 mV while GABA_AR-mediated PSCs reversed at –60 mV. Miniature Inhibitory and Excitatory PSCs (mIPSCs and mEPSCs) were collected in the presence of TTX (1 μ M, Tocris) at a holding potential of +10 mV and of –60 mV respectively. Recordings were also performed at +40 mV to isolate NMDA-R-mediated EPSCs. For current clamp recordings, the intracellular solution contained: 130 mM K-methylSO₄, 5 mM KCl, 5 mM NaCl, 10 mM HEPES, 2.5 mM Mg-ATP, and 0.3 mM GTP. No correction for liquid junction potential was applied. The osmolarity was 265–275 mOsm, pH 7.3. Recordings were analyzed using the MiniAnalysis software (Synaptosoft).

Morphological analysis

Slices were processed for the detection of Neurobiotin-filled neurons as follows: briefly, slices were fixed overnight at 4 °C in Antigenfix (Diapath). After several rinses in PBS containing 0.3% Triton X-100 (PBST), slices were incubated overnight at room temperature in 1/1000 streptavidin coupled to cy3 diluted in PBST. Slices were rinsed in PBS before mounting between slide and coverslide in Fluoromount (Southern Biotech). Post-hoc analysis was performed using a confocal microscope. Stacks of optical sections were collected for computer-assisted neuron reconstructions.

Eighteen neurons were reconstructed with a computer-assisted system attached to a microscope (NeuroLucida software, MicroBrightfield). Morphological variables included: total dendritic and axonal lengths, total dendritic and axonal surfaces, and total number of dendritic and axonal terminals. The total surface of dendrites or axons (branched structures) is an estimated value calculated by the software. The total length of dendrites or axons is the sum of the lengths of all the branches. We also performed a Sholl analysis in order to determine the distribution of the number of dendritic intersections with circles of increasing radius (20 μ m steps) centred at the cell's soma.

For each neuron, the linear density of dendritic protrusions was calculated in a 20 μ m segment length from second order dendritic branches.

Mice for inducible genetic fate mapping

Double-homozygous Mash1BAC^{CreER/CreER/RCE:LoxP^{+/+}} (Miyoshi et al., 2010) male mice were crossed with 7- to 8-week-old wild-type Swiss females (C.E Janvier, France) for

offspring production. To induce CreER activity, we administered a tamoxifen solution (Sigma, St. Louis, MO) by gavaging (force-feeding) pregnant mice with a silicon-protected needle (Fine Science Tools, Foster City, CA). We used 2 mg of tamoxifen solution per 30 g of body weight prepared at 10 mg/ml in corn oil (Sigma). Pregnant females crossed with Mash1BAC^{CreER/CreER}/RCE:LoxP^{+/+} males were gavaged at E 11.5 and E18.5, in order to label early and late expressing Mash1 precursors respectively, in the embryos named Mash1CreERTM; RCE:LoxP mice (Picardo et al., 2011).

Statistical analysis

Experimental values are given as mean \pm S.E.M. Statistical significance between means was calculated using Student's t test or Mann & Whitney Rank Sum Test in the case where normality test failed. $p < 0,05$ was considered significant.

Results

GABAergic interneurons are involved in SPAs

We hypothesized that SPAs could be a central step for the maturation of interneurons given that GABAergic transmission is essential for the generation of GDPs (Ben Ari et al., 1989; Bonifazi et al., 2009; Garaschuk et al., 1998; Sipila et al., 2005) and that SPAs occur just before their emergence (Allene et al., 2008; Crepel et al., 2007). However, it remains unknown whether SPAs similarly involve glutamatergic and GABAergic neurons. In order to address this issue, we have quantified the proportion of GABAergic cells producing calcium plateaus. We focused on P1–5 and imaged the CA3 hippocampal region of GAD67-Green Fluorescent Protein- Knock-In (GAD67-GFP-KI) mouse slices in which GABAergic cells are labelled with GFP (Tamamaki et al., 2003). The contour maps corresponding to GFP positive neurons were superimposed on the distribution of neurons producing SPAs (see methods, Fig. 1). We found that cells involved in coordinated activity patterns near birth (P1) comprise mainly GABAergic neurons, with around 25 % of interneurons involved either in SPAs or GDPs (16 \pm 4% and 9 \pm 9% respectively, $n=6$ slices, Fig. 1B2) compared to less than 5% of pyramidal cells involved in any type of activity (Fig. 1B2). Later, in both neuronal populations, the fraction of cells involved in coordinated activities increases across the first postnatal week (Fig. 1B2). Specifically focusing our analysis on SPAs, we found that half of the SPA-neurons were GABAergic at P1 (51 \pm 9% of SPA-cells were GFP+ at P1, $n=6$ slices, Fig. 1B1) and that the participation of interneurons to SPAs declined abruptly within a few days (20 \pm 12% of SPA-cells were GFP+ at P3, $n=5$ slices, Fig. 1B1). Ultimately, at P7, almost all GABAergic neurons participated in GDPs (87 \pm 7% of GFP+ cells were GDP neurons at P7, $n=6$ slices). Targeted patch-clamp recordings confirmed that GFP positive SPA neurons indeed produced the characteristic membrane potential oscillations associated with SPAs (Fig. 1D). Moreover, in a few cases, we observed dye labelling of two interneurons as well as spikelets, indicating a putative gap-junction coupling between SPA-cells (Fig. 1C, D2). In contrast, in more mature slices (P5), almost 90% of SPA cells were glutamatergic neurons (on average: 11 \pm 3% SPA cells were GFP+; $n=9$ slices Fig. 1B1). We conclude that GABAergic neurons participate in the production of SPAs at different developmental stages with their involvement decreasing overtime until the end of the first postnatal week, when almost all GABAergic neurons are involved in GDPs.

SPA-cells develop into GDP-cells as the hippocampal network matures

Given that developmental cell loss has been reported at early postnatal stages (Buss and Oppenheim, 2004), SPAs could be selectively expressed by transient neuronal populations, or alternatively be a transient activity step occurring during the maturation of most neurons. In order to directly address this question, we have performed daily multineuron calcium

imaging following the same neuronal populations in the CA3 region of organotypic hippocampal slices prepared from GAD67-GFP-KI mice. To this end, we have designed an experimental procedure to avoid culture contamination through repetitive imaging sessions using multibeam two-photon calcium microscopy (see Methods). Organotypic hippocampal slice cultures provide a robust model to chronically study the maturation of coherent activity patterns since they produce similar network dynamics as previously observed in acute slices (Crepel et al., 2007). Indeed, spontaneous network dynamics similar to GDPs in terms of both their calcium dynamics and pharmacological characteristics (Crepel et al., 2007) could be recorded in every organotypic slice (n=12 slices): they consisted of fast calcium events occurring simultaneously in many neurons within one movie frame (Crepel et al., 2007) at 0.04/- 0.01 Hz (n=12 slices, Fig. 2). These dynamics were dependent on the excitatory actions of GABA as they were blocked by the selective NKCC1 antagonist bumetanide (In bumetanide (10 μ M), the frequency and amplitude of GDPs decreased to 11 +/- 11% and 20 +/- 20% of control respectively, n=5 slices, p<0.05, data not shown). Calcium plateaus corresponding to SPAs could also be recorded and involved 27 +/- 6% of imaged neurons on average (n=12 slices). We next focused on the fate of individual SPA-cells and surprisingly after one day found that many SPA-cells stopped producing calcium plateaus and participated in GDPs. Indeed, after one day in culture, the fraction of SPA-cells involved in GDPs significantly increased whereas the fraction of SPA-cells still producing plateaus decreased (to 56 +/- 5% and 11 +/- 1% respectively (n=4 slices, n=520 neurons), Fig. 2). If we focus our analysis on the GABAergic neuron population, we find that 40% of GFP positive SPA-cells (i.e. SPA-interneurons) transit to the GDP stage within one day (39 +/- 13%, n=4 slices, n=96 neurons, Fig. 2) whereas the fraction of SPA-interneurons still producing plateaus decreased by more than 60% (to 39 +/- 8% respectively). In addition, almost all interneurons starting to participate in GDPs on the second imaging session had been involved in SPAs on the previous day (86% of newly detected GFP+ GDP cells originate from GFP+ SPA cells, n=44 GFP+ cells). We therefore conclude that a portion of GDP-interneurons originate from SPA-interneurons and that the fate of many SPA-interneurons is to start participating in GDPs as development proceeds.

GABAergic SPA- and GDP-cells possess variable morphologies with SPA-interneurons displaying a larger soma size and dense membrane protrusions

We next wondered whether the transition between SPA- and GDP- activity patterns may be paralleled by changes in the morpho-physiological properties of GABAergic interneurons. To analyze morphological features, GABAergic SPA- and GDP-cells were targeted for neurobiotin-filling based on their calcium kinetics, first at P4, a stage when both patterns are expressed in comparable proportions within the CA3 hippocampal network. GFP-positive cells were specifically targeted and immunohistochemically processed *post hoc*. Out of 53 morphologically recovered interneurons, 9 SPA- and 9 GDP-interneurons were reconstructed for morphometric analysis (Fig. 3). Although at P4, SPA- and GDP-interneuron populations were quite morphologically immature, they still displayed considerable diversity with various cell body locations and different dendritic and axonal arborisation patterns (Fig. 3). The soma of SPA- and GDP-interneurons was located in stratum oriens (in 22 and 33% of the cases, respectively, n=53), radiatum (22% and 55%, respectively, n=53) or pyramidale (55 and 11%, respectively, n=53). Around half of interneurons in both groups displayed a very small axon if any. Among the interneurons with a more developed axonal arborisation we observed two SPA-interneurons with putative perisomatic, basket-like axonal morphology (one is reconstructed, Fig. 3) and two putative long-range SPA-interneurons (Fig. 3). Concerning GDP-interneurons we found four cells with putative perisomatic, basket-like axonal morphology (one is reconstructed, Fig. 3) and five cells with more local and less arborized axons (Fig 3). The presence of basket-like interneurons in both groups, suggests that this interneuron subtype likely transits from a

SPA to a GDP state. We also quantified dendritic and axonal lengths, nodes and surfaces (Table) and performed a sholl analysis (data not shown). In comparing SPA- and GDP-interneurons, none of the parameters measured were significantly different. Even within the same putative morphological subgroup of basket-like interneurons, there was no striking significant difference between cell morphologies (Fig. 3). However, SPA-interneurons could be distinguished from GDP-interneurons by two features. First, they on average exhibited a significantly larger soma size ($165 \pm 21 \mu\text{m}^2$, $n=9$ SPA-cells vs. $105 \pm 10 \mu\text{m}^2$, $n=9$ GDP-cells, $p < 0.05$, see Table and Fig. 3B, D). Second, their dendrites (and also sometimes their soma, Fig. 3C, D) tended to be covered with numerous protrusions. The linear density of these processes was quantified (see methods) and on average significantly higher in SPA- vs. GDP-interneurons ($0.25 \pm 0.05/\mu\text{m}$, $n=22$ cells and $0.14 \pm 0.05/\mu\text{m}$, $n=16$ cells, respectively, $p < 0.05$, Fig. 3D). This is surprising given that, in contrast to glutamatergic cells and with a few exceptions, the dendritic arbor of most GABAergic interneurons is aspiny.

We conclude that both SPA and GDP-interneuron populations likely comprise a variety of morphological cell types that are largely at similar stages of dendritic and axonal development. However, SPA interneurons display certain characteristics, including a larger cell body and membrane protrusions.

While different subtypes of GABAergic SPA-cells display similar intrinsic electrophysiological properties, firing diversity only emerges in GABAergic GDP-cells

We next targeted SPA- and GDP-interneurons at P4 for current and voltage clamp recordings and characterized their intrinsic and synaptic electrophysiological properties. As expected (Crepel et al., 2007), in current clamp mode, at resting membrane potential (V_{rest}), SPA-interneurons displayed recurrent membrane potential oscillations which are not affected by synaptic transmission blockade using GABAA- AMPA- and NMDA-receptor antagonists ($10 \mu\text{M}$ bicuculline, $10 \mu\text{M}$ NBQX, $40 \mu\text{M}$ D-APV, $n=14$ cells, Fig. 4). Most GDP-interneurons were also spontaneously firing at V_{rest} in the presence of synaptic blockers, however, in contrast to SPA-interneurons, they tonically fired action potentials (Fig. 4). We also investigated the firing patterns of interneurons in response to depolarizing and hyperpolarizing current steps. We found that almost all SPA-interneurons displayed a strongly adapting firing pattern (72%, $n=11$ SPA-interneurons, Fig. 4) whereas GDP-interneurons presented a variety of firing patterns (Fig. 4) that could be classified, according to the Petilla nomenclature (Ascoli et al., 2008) as, fast spiking ($n=12$), non-adapting ($n=2$), adapting ($n=4$), irregular spiking ($n=2$) or stuttering ($n=1$). Basket-like GDP interneurons presented a fast spiking pattern whereas spiking in basket-like SPA-cells was strongly delayed and adapting (Fig. 4). In addition, resting membrane potential (V_{rest}) and action potential (AP) amplitude and duration were significantly different between SPA and GDP interneurons: SPA-cells displayed a more depolarized V_{rest} and a broader and smaller AP (Table), all features indicating a rather immature stage of development (Doischer et al., 2008; Moody and Bosma, 2005; Okaty et al., 2009). Moreover and in agreement with the morphological results concerning the cell body size, the membrane resistances (R_m) and capacitances (C_m) of SPA- and GDP-interneurons were significantly different. SPA-interneurons displayed smaller membrane resistances and higher membrane capacitances when compared to GDP-interneurons (see Table). In contrast, the fraction of SPA- and GDP-interneurons displaying an h-current evoked by hyperpolarizing current steps was not different (83%, $n=7$ neurons and 90%, $n=20$ neurons, respectively).

Synaptic inputs differ between SPA- and GDP- interneurons

Since GDPs are synapse-driven network events whereas SPAs do not depend on synaptic transmission for their generation, we hypothesized that GDP-interneurons receive more

synaptic inputs than SPA-interneurons. As a first step towards addressing this issue, at P4 we recorded spontaneous and miniature Excitatory and Inhibitory Postsynaptic Currents (sEPSC/sIPSCs and mEPSC/mIPSCs respectively) in SPA- or GDP-interneurons. Surprisingly, on average, the frequency and kinetics of spontaneous and miniature EPSCs and IPSCs impinging onto SPA- and GDP-interneurons were not significantly different (see Table). However, the average amplitude of miniature events (mEPSCs and mIPSCs) received by SPA-interneurons was significantly larger than that received by GDP-interneurons (see Table and Fig. 5). These large average amplitude values can be attributed to the higher occurrence of large amplitude PSCs in SPA-interneurons compared to GDP interneurons as revealed by PSCs amplitude distribution histograms. Histograms plotting the distribution of mIPSC/mEPSCs amplitudes of both SPA- and GDP-interneurons were unimodal but skewed towards larger events in SPA- cells (Kolmogorov-Smirnov, $p < 0.05$). Accordingly, mEPSCs and mIPSCs received by SPA-interneurons displayed a higher variability as measured by their larger standard deviation (SD= 27 vs. 6, for mEPSCs in SPA- vs. GDP-cells, and SD=34 vs. 21, for mIPSCs in SPA- vs. GDP-cells, Fig. 5). We conclude that SPA-cells receive synaptic inputs of higher amplitude variability with, significantly higher average amplitude values than GDP-cells.

Cells mature during the SPA stage in accordance with their birthdate

At P4, SPA-interneurons share characteristic morpho-physiological properties that include membrane protrusions, immature firing patterns and high amplitude synaptic inputs. We next asked whether these properties could still be found in the few remaining SPA-interneurons at later postnatal stages (P7). To address this issue, we targeted 5 SPA-interneurons at P7 and found that their morpho-physiological properties were not significantly different from SPA-interneurons at P4 with the exception that there was a global increase in the size of neurons (Fig. 6). Hence, if the average cell body area of all neurons, including SPA-cells, increased between P4 and P7 (by 120% as estimated from the area of imaged cell contours), the soma of SPA cells remained significantly larger than that of GDP cells at P7 ($207 \pm 4 \mu\text{m}^2$ (n=3) and $143 \pm 19 \mu\text{m}^2$ (n=4) respectively, $p < 0.05$). Therefore we conclude that the morpho-physiological features of SPA-cells are not likely to be determined by the developmental stage of the network they are embedded into but rather reflect the intrinsic developmental stage of the SPA-cell. To further confirm this hypothesis, we have analyzed the involvement of interneurons in SPAs according to their birth date. We hypothesized that Early Generated Interneurons (EG-Ins) could have already achieved the SPA to GDP transition at P3 when GABAergic cells are still more involved in SPAs than GDPs, whereas Late Generated Interneurons (LG-Ins) (Picardo et al., 2011) would be more likely to be still involved in SPAs later at P7, when the majority of interneurons have transitioned to a GDP stage. We therefore used an inducible genetic fate mapping strategy to label interneurons according to their time of embryonic origin. We combined the *Mash1BAC-CreER* driver with the *RCE:loxP* reporter (Picardo et al., 2011) and through tamoxifen administration at E11.5 and E18.5, two subpopulations of CA3 EG-Ins and LG-Ins, which are specifically derived from the E11.5 and E18.5 caudal ganglionic eminence respectively, are labelled by EGFP (see details in methods). At P3, EG-Ins were targeted for electrophysiological recordings. Unfortunately, for unknown reasons, EG-Ins could not be efficiently labelled with the calcium-permeable indicator used here (Fura2-AM) (Picardo et al., 2011) which precluded determining their spontaneous activity based on the analysis of their spontaneous calcium events. Note that all EG-Ins, recorded both in current- or voltage-clamp modes already received GDPs, while less than 20 % of the entire GABAergic cell population was involved in GDPs (18%, n=143 neurons, 9 slices, Fig. 7A). At P7, calcium imaging was performed to detect SPA-cells in hippocampal slices where E18.5 caudal ganglionic eminence-derived interneurons were specifically labelled with EGFP (Fig. 7B). We found that LG-Ins were more likely to be still producing SPAs at P7 than the overall

interneuron population, as 43% of active LG-Ins were detected as SPA-cells (n=7 cells, Fig. 7B) while SPA-cells accounted for less than 20 % of all GABAergic neurons (16 %, n=91 neurons, 6 slices, Fig. 7B3). We conclude that EG-Ins already produce GDPs at a period dominated by SPAs whereas LG-Ins are involved in SPAs over a protracted period of interneuron maturation.

Discussion

We have examined the correlation between the development of cellular properties in GABAergic interneurons and their participation in spontaneous patterned activities by combining imaging with electrophysiology, morphology and inducible genetic fate-mapping. We find that in parallel to the sequential evolution from SPAs to GDPs, the properties of GABAergic cells mature at anatomical, intrinsic electrophysiological and synaptic levels. This demonstrates that events at the network and cellular level are most likely modulated by reciprocal feedback on one another. However, interneuron involvement in SPAs or GDPs is dependent on their birth: while the morpho-physiological characteristics of SPA-interneurons are constant at both early and late postnatal stages, late generated interneurons tend to produce SPAs at later developmental periods and early generated ones are more likely to receive GDPs during early postnatal periods. These results support a strong correlation between circuit and single-cell maturation.

Within the same network, developing neurons are heterogeneously involved in different activity patterns

Although network oscillations produced by a specific cellular mechanism dominate at specific stages of development (Allene and Cossart, 2010; Blankenship and Feller, 2010), several types of spontaneous activities co-exist within the same network as development progresses. In addition, many cells are silent and thus do not participate in any form of synchronous activity. The present study focuses on a narrow time period of postnatal development that corresponds to the switch from SPA- to GDP-dominated hippocampal networks (Crepel et al., 2007). Considering all types of neurons, including glutamatergic cells, we found that a majority of SPA-cells transit to GDPs over a one-day period in cultures. This transition may occur at a different rate *in vivo*. By contrast and in agreement with the fact that interneuron genesis occurs over several days, less than half of the SPA-interneurons transit to GDPs within one culture day. Moreover, since we are technically unable to follow the fate of individual cells over longer time periods, we cannot be certain that all interneurons make the SPA to GDP transition. Indeed, given the abrupt rise in the fraction of GDP interneurons observed between P1 and P3, some interneuron subtypes may directly become GDP contributors. Despite this caveat, many interneurons undergo this transition as a majority (86%) of the newly identified GDP-interneurons in slice cultures originated from cells involved in SPAs on the previous day. Furthermore, from a mechanistic standpoint, since the occurrence of GDPs actively terminates the calcium plateaus associated with SPAs (Crepel et al., 2007), persistence of these long calcium transients may ultimately trigger apoptotic programs (Golbs et al., 2011).

Cellular morpho-physiological correlates of SPA activity

Significant differences in the maturation of the intrinsic electrophysiological properties were observed when comparing SPA- and GDP-interneurons. Independent of their morphological subtype, all SPA-interneurons displayed broader and smaller action potentials, together with strongly adapting firing patterns and a depolarized V_{rest} . All these properties have been attributed to variations in the expression and spatial distribution of voltage-gated channels in immature cells (Doischer et al., 2008; Moody and Bosma, 2005). In addition, SPA-cells display a higher averaged capacitance value, which likely reflects a larger neuronal surface

(Tyzio et al., 2003) due to a larger soma size and higher membrane protrusion density. The larger soma of SPA-interneurons can also account for their lower input resistance.

Membrane protrusions and in particular filopodia are a hallmark of developing neurons during migration and morphogenesis (Guerrier et al., 2009). However, we were not able to classify protrusions into a specific group since some resembled filopodia-like processes whereas others appeared more spine-like. Interestingly, the adult interneuron population is with few exceptions well known for the absence of spines in most subtypes (Freund and Buzsáki, 1996). Nonetheless, somatic protrusions in developing interneurons may, as recently proposed (Guerrier et al., 2009), contribute to the arrest of neuronal migration. The elevated intracellular chloride concentration present in immature neurons could result in osmotic pressure that acts to increase somal volume while the high intracellular calcium levels associated with SPAs could favour protrusion motility. Consistent with these ideas, both the end of interneuron migration as well as the emergence of SPAs is shown to depend on chloride and calcium intracellular concentrations (Bortone and Polleux, 2009; Crepel et al., 2007).

Although future studies will be required to determine the exact function of these protrusions, it may be the case that they promote the maturation of synaptic inputs onto interneurons. In general, immature synaptic inputs give rise to low frequency and slow kinetics mPSCs that favor GABAergic inputs over glutamatergic ones (Hennou et al., 2002; Tyzio et al., 1999; Wang and Kriegstein, 2008). Unexpectedly, except for the decay of mEPSCs, which was faster in SPA-cells, we could not find any significant difference in the frequency or kinetics of miniature and spontaneous PSCs between interneurons involved in SPAs or GDPs. This indicates that the number, distribution and subunit composition of glutamatergic and GABAergic synaptic inputs impinging onto SPA- and GDP-interneurons is likely to be comparable. However, given the diversity of the GABAergic interneuron population we cannot exclude that significant differences do not exist until we are able to restrict our comparisons to interneurons of the same subtype. This remains a challenging task given the late development of classic interneuron markers and the fact that different subtypes can only be distinguished after these events have been completed.

SPA- and GDP- interneurons however differed in their PSCs amplitude distributions, with SPA interneurons possessing a higher proportion of miniature events with large amplitudes. These large amplitude PSCs raise several unsolved questions regarding both the mechanisms of their generation, as well as their function. Given the fact that large amplitude events occur similarly for GABAergic and glutamatergic inputs, the mechanism generating them may well be postsynaptic in origin. However, we cannot exclude that SPA-interneurons are not selectively innervated by specific presynaptic glutamatergic and GABAergic partners, that for example share the same temporal embryonic origin (Deguchi et al., 2011; Yu et al., 2009).

We can thus conclude that the transition from a SPA- to a GDP- activity pattern has several morpho-physiological correlates at the cellular level and inaugurates the expression of physiological diversity in GABAergic interneurons. Whether the SPA to GDP transition is causally mediating this morpho-physiological evolution remains to be determined by specific interference experiments.

Postnatal morpho-physiological development of interneurons: activity vs. intrinsic programs?

The previously presented results raise the question as to whether the development of cortical interneurons is more influenced by activity or by intrinsic genetic programs (Cossart, 2011; Fishell and Rudy, 2011). Previous studies suggest that the adult morpho-physiological

phenotype of cortical interneurons is strongly predetermined by their spatio-temporal embryonic origins (Batista-Brito and Fishell, 2009; Butt et al., 2005; Corbin and Butt, 2011; Tricoire et al., 2011; Xu et al., 2004), while early and late postnatal activities respectively determine their final position and morphological development (De Marco Garcia et al., 2011). One possible interpretation of our findings is that the maturation of all interneurons is dictated by their birthdate and is independent of their subtype, spatial origin or the ambient network activities that they experience. This idea is however seemingly at odds with earlier observations noting that early and late born CGE-derived interneurons enter the cortex and uniformly occupy the superficial laminae independent of their birthdate (Miyoshi et al., 2010). However, these latter findings pertain to the cortex rather than the hippocampus where the laminar fate of late born neurons can be altered if network activity is disrupted during development (De Marco Garcia et al., 2011). Perhaps the correct conclusion is that some aspects of interneuron development such as the SPA to GDP transition are generic, while others such as laminar position reflect intrinsic differences within distinct subclasses. Regardless of these differences, it seems clear that genetic programs initiated at birth are crucial in dictating the timing at which developing neurons synaptically integrate into functional cortical circuits (Deguchi et al., 2011; Petrovic and Hummel, 2008). In fact, the present results suggest a mechanistic basis for the previously described selective wiring between temporally-matched cell populations (Deguchi et al., 2011): cells generated at the same time will likely display at critical points of development similar firing dynamics, independent of their subtype, and as such be predisposed to wire together. Importantly these findings highlight that despite the natural desire to discriminate between intrinsic genetic programs and activity, the contributions of each are inherently intertwined.

To conclude, we have shown that the SPA to GDP transition, which is likely to occur in several interneuron subtypes, has significant morpho-physiological correlates. Since this sequence is shared across developing cortical structures (Allene and Cossart, 2010), this observation may well be generalizable. A better understanding of the parameters that govern the SPA to GDP switch should ultimately help us understand the etiology of the developmental brain disorders classified as interneuropathies.

Acknowledgments

We thank Pr. Jane Johnston for providing the *Mash1*^{CreERTM} mouse. We thank Drs. A. Baude, S. Feldt and V. Villette for critical comments. Research in the Cossart group was supported by grants from the European Research Council (ERC FP7 Young Investigators #242852), the Fondation pour la Recherche Medicale (Equipe FRM 2008), the Fondation Bettencourt Schueller, I.N.S.E.R.M., the Ville de Marseille and Region P.A.C.A. and the F.R.C. Drs. R. Cossart and A. Baude are funded by the C.N.R.S. C. Allene was funded by a fellowship from the F.R.M.. Research in the Fishell laboratory is supported by the National Institutes of Health (NIH RO1 grants R01MH071679 and R01NS039007), as well as generous support from NYSTEM and the Simons Foundation. G.M. is supported by a grant from the National Alliance for Research on Schizophrenia and Depression.

Reference List

- Allene C, Cattani A, Ackman JB, Bonifazi P, Aniksztejn L, Ben-Ari Y, Cossart R. Sequential generation of two distinct synapse-driven network patterns in developing neocortex. *J Neurosci.* 2008; 28:12851–12863. [PubMed: 19036979]
- Allene C, Cossart R. Early NMDA receptor-driven waves of activity in the developing neocortex: physiological or pathological network oscillations? *J Physiol.* 2010; 588:83–91. [PubMed: 19917570]
- Ascoli GA, et al. Petilla terminology: nomenclature of features of GABAergic interneurons of the cerebral cortex. *Nat Rev Neurosci.* 2008; 9:557–568. [PubMed: 18568015]
- Batista-Brito R, Fishell G. The developmental integration of cortical interneurons into a functional network. *Curr Top Dev Biol.* 2009; 87:81–118. [PubMed: 19427517]

- Ben Ari Y, Cherubini E, Corradetti R, Gaiarsa JL. Giant synaptic potentials in immature rat CA3 hippocampal neurones. *J Physiol*. 1989; 416:303–325. [PubMed: 2575165]
- Ben-Ari Y, Gaiarsa JL, Tyzio R, Khazipov R. GABA: a pioneer transmitter that excites immature neurons and generates primitive oscillations. *Physiol Rev*. 2007; 87:1215–1284. [PubMed: 17928584]
- Blankenship AG, Feller MB. Mechanisms underlying spontaneous patterned activity in developing neural circuits. *Nat Rev Neurosci*. 2010; 11:18–29. [PubMed: 19953103]
- Bonifazi P, Goldin M, Picardo MA, Jorquera I, Cattani A, Bianconi G, Represa A, Ben-Ari Y, Cossart R. GABAergic hub neurons orchestrate synchrony in developing hippocampal networks. *Science*. 2009; 326:1419–1424. [PubMed: 19965761]
- Bortone D, Polleux F. KCC2 expression promotes the termination of cortical interneuron migration in a voltage-sensitive calcium-dependent manner. *Neuron*. 2009; 62:53–71. [PubMed: 19376067]
- Buss RR, Oppenheim RW. Role of programmed cell death in normal neuronal development and function. *Anat Sci Int*. 2004; 79:191–197. [PubMed: 15633457]
- Butt SJ, Fuccillo M, Nery S, Noctor S, Kriegstein A, Corbin JG, Fishell G. The temporal and spatial origins of cortical interneurons predict their physiological subtype. *Neuron*. 2005; 48:591–604. [PubMed: 16301176]
- Catalano SM, Shatz CJ. Activity-dependent cortical target selection by thalamic axons. *Science*. 1998; 281:559–562. [PubMed: 9677198]
- Corbin JG, Butt SJ. Developmental mechanisms for the generation of telencephalic interneurons. *Dev Neurobiol*. 2011; 71:710–732. [PubMed: 21485015]
- Cossart R. The maturation of cortical interneuron diversity: how multiple developmental journeys shape the emergence of proper network function. *Curr Opin Neurobiol*. 2011; 21:160–168. [PubMed: 21074988]
- Crepel V, Aronov D, Jorquera I, Represa A, Ben-Ari Y, Cossart R. A parturition-associated nonsynaptic coherent activity pattern in the developing hippocampus. *Neuron*. 2007; 54:105–120. [PubMed: 17408581]
- De Marco Garcia NV, Karayannis T, Fishell G. Neuronal activity is required for the development of specific cortical interneuron subtypes. *Nature*. 2011; 472:351–355. [PubMed: 21460837]
- Deguchi Y, Donato F, Galimberti I, Cabuy E, Caroni P. Temporally matched subpopulations of selectively interconnected principal neurons in the hippocampus. *Nat Neurosci*. 2011; 14:495–504. [PubMed: 21358645]
- Doischer D, Hosp JA, Yanagawa Y, Obata K, Jonas P, Vida I, Bartos M. Postnatal differentiation of basket cells from slow to fast signaling devices. *J Neurosci*. 2008; 28:12956–12968. [PubMed: 19036989]
- Fishell G, Rudy B. Mechanisms of inhibition within the telencephalon: “where the wild things are”. *Annu Rev Neurosci*. 2011; 34:535–567. [PubMed: 21469958]
- Freund TF, Buzsáki G. Interneurons of the hippocampus. *Hippocampus*. 1996; 6:347–470. [PubMed: 8915675]
- Garaschuk O, Hanse E, Konnerth A. Developmental profile and synaptic origin of early network oscillations in the CA1 region of rat neonatal hippocampus. *J Physiol (Lond)*. 1998; 507:219–236. [PubMed: 9490842]
- Golbs A, Nimmervoll B, Sun JJ, Sava IE, Luhmann HJ. Control of programmed cell death by distinct electrical activity patterns. *Cereb Cortex*. 2011; 21:1192–1202. [PubMed: 20966045]
- Guerrier S, Coutinho-Budd J, Sassa T, Gresset A, Jordan NV, Chen K, Jin WL, Frost A, Polleux F. The F-BAR domain of srGAP2 induces membrane protrusions required for neuronal migration and morphogenesis. *Cell*. 2009; 138:990–1004. [PubMed: 19737524]
- Hennou S, Khalilov I, Diabira D, Ben Ari Y, Gozlan H. Early sequential formation of functional GABA(A) and glutamatergic synapses on CA1 interneurons of the rat foetal hippocampus. *Eur J Neurosci*. 2002; 16:197–208. [PubMed: 12169102]
- Miyoshi G, Hjerling-Leffler J, Karayannis T, Sousa VH, Butt SJ, Battiste J, Johnson JE, Machold RP, Fishell G. Genetic fate mapping reveals that the caudal ganglionic eminence produces a large and diverse population of superficial cortical interneurons. *J Neurosci*. 2010; 30:1582–1594. [PubMed: 20130169]

- Moody WJ, Bosma MM. Ion channel development, spontaneous activity, and activity-dependent development in nerve and muscle cells. *Physiol Rev.* 2005; 85:883–941. [PubMed: 15987798]
- Okaty BW, Miller MN, Sugino K, Hempel CM, Nelson SB. Transcriptional and electrophysiological maturation of neocortical fast-spiking GABAergic interneurons. *J Neurosci.* 2009; 29:7040–7052. [PubMed: 19474331]
- Petrovic M, Hummel T. Temporal identity in axonal target layer recognition. *Nature.* 2008; 456:800–803. [PubMed: 18978776]
- Pfeffer CK, Stein V, Keating DJ, Maier H, Rinke I, Rudhard Y, Hentschke M, Rune GM, Jentsch TJ, Hubner CA. NKCC1-dependent GABAergic excitation drives synaptic network maturation during early hippocampal development. *J Neurosci.* 2009; 29:3419–3430. [PubMed: 19295148]
- Picardo MA, Guigue P, Bonifazi P, Batista-Brito R, Allene C, Ribas A, Fishell G, Baude A, Cossart R. Pioneer GABA Cells Comprise a Subpopulation of Hub Neurons in the Developing Hippocampus. *Neuron.* 2011; 71:695–709. [PubMed: 21867885]
- Sipila ST, Huttu K, Soltesz I, Voipio J, Kaila K. Depolarizing GABA acts on intrinsically bursting pyramidal neurons to drive giant depolarizing potentials in the immature hippocampus. *J Neurosci.* 2005; 25:5280–5289. [PubMed: 15930375]
- Stoppini L, Buchs PA, Muller D. A simple method for organotypic cultures of nervous tissue. *J Neurosci Methods.* 1991; 37:173–182. [PubMed: 1715499]
- Tamamaki N, Yanagawa Y, Tomioka R, Miyazaki J, Obata K, Kaneko T. Green fluorescent protein expression and colocalization with calretinin, parvalbumin, and somatostatin in the GAD67-GFP knock-in mouse. *J Comp Neurol.* 2003; 467:60–79. [PubMed: 14574680]
- Tricoire L, Pelkey KA, Erkkila BE, Jeffries BW, Yuan X, McBain CJ. A blueprint for the spatiotemporal origins of mouse hippocampal interneuron diversity. *J Neurosci.* 2011; 31:10948–10970. [PubMed: 21795545]
- Tyzio R, Ivanov A, Bernard C, Holmes GL, Ben Ari Y, Khazipov R. The Membrane Potential of CA3 Hippocampal Pyramidal Cells During Postnatal Development. *J Neurophysiol.* 2003; 90:2964–72. [PubMed: 12867526]
- Tyzio R, Represa A, Jorquera I, Ben Ari Y, Gozlan H, Aniksztejn L. The establishment of GABAergic and glutamatergic synapses on CA1 pyramidal neurons is sequential and correlates with the development of the apical dendrite. *J Neurosci.* 1999; 19:10372–10382. [PubMed: 10575034]
- Wang DD, Kriegstein AR. GABA regulates excitatory synapse formation in the neocortex via NMDA receptor activation. *J Neurosci.* 2008; 28:5547–5558. [PubMed: 18495889]
- Wei W, Feller MB. Organization and development of direction-selective circuits in the retina. *Trends Neurosci.* 2011; 12:638–45. [PubMed: 21872944]
- Xu HP, Furman M, Mineur YS, Chen H, King SL, Zenisek D, Zhou ZJ, Butts DA, Tian N, Picciotto MR, Crair MC. An instructive role for patterned spontaneous retinal activity in mouse visual map development. *Neuron.* 2011; 70:1115–1127. [PubMed: 21689598]
- Xu Q, Cobos I, De La CE, Rubenstein JL, Anderson SA. Origins of cortical interneuron subtypes. *J Neurosci.* 2004; 24:2612–2622. [PubMed: 15028753]
- Yu YC, Bultje RS, Wang XQ, Shi SH. Specific synapses develop preferentially among sister excitatory neurons in the neocortex. *Nature.* 2009; 458:501–5U3. [PubMed: 19204731]

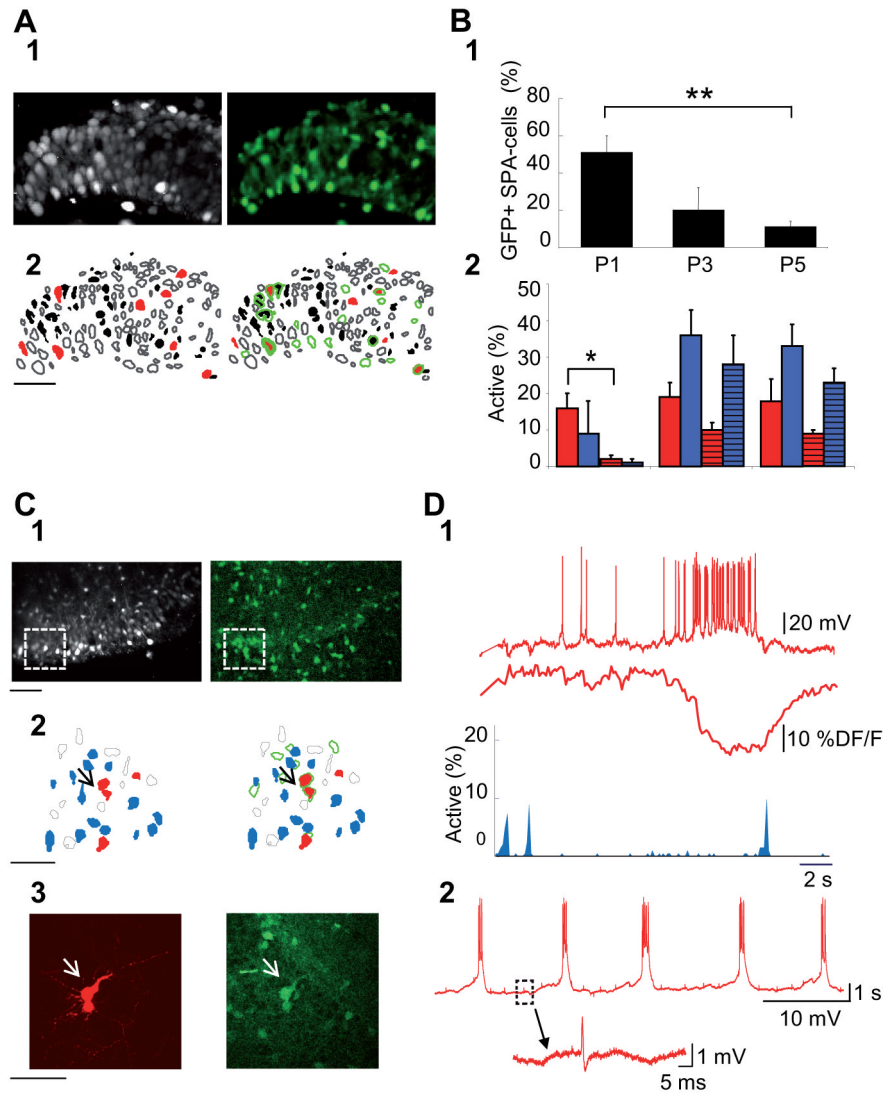


Figure 1. GABAergic neurons are preferentially involved in SPAs at early postnatal stages (P0–5)

A1. Two-photon calcium fluorescence image from the CA3 region of a P1 GAD67-KI-GFP mouse (left) and the GFP signal from the same field (right). A2. Automatically detected contours of the cells (left) from the calcium fluorescence image (A1) and overlap of this contour map with that of GFP positive cells (right). Silent cells: open contours, cells producing calcium spikes: black filled contours, SPA-cells: red filled contours, GFP positive cells: green open contours. Note that in this case, half of the SPA cells are GFP positive. B.1 Histogram indicating the fraction of SPA-cells that are GFP positive at three time points: P1, P3 and P5. B.2 Histogram indicating the fraction of interneurons (full colored bars) and of pyramidal cells (striped bars) involved in SPAs (red) or in GDPs (blue) relative to the total interneuron or pyramidal cell population, respectively, as a function of time. C1. Two-photon calcium fluorescence image from the CA3 region of a P5 GAD67-KI-GFP mouse (left) and the GFP signal from the same field (right). C2. Contour map of the imaged cells (left) from the dashed area indicated in (C1) and superimposition with the GFP positive cell contour map (right). Silent cells: open contours, SPA-cells: red filled contours, GDP-cells: blue filled contours, GFP positive cells: green open contours. C3. High magnification image

of a neurobiotin filled SPA-interneuron (arrows, left) and the corresponding GFP confocal image (right) suggests that the targeted SPA-interneuron is coupled with an other interneuron by a gap junction. D1. Patch clamp recording in current clamp mode at resting membrane potential (0pA, upper red trace) of the targeted SPA-interneuron in (C.), the corresponding calcium fluorescence trace (middle) and histogram (bottom) indicating the fraction of active cells as a function of time: each blue peak represents a GDP. Note that the occurrence of a GDP switches off the calcium plateau as previously shown (Crepel et al., 2007). D2. Recurrent membrane potential oscillations characteristic of SPA-cells from the same SPA-interneuron that above further supports gap junction coupling by the presence of spikelets shown on an expanded time scale below.

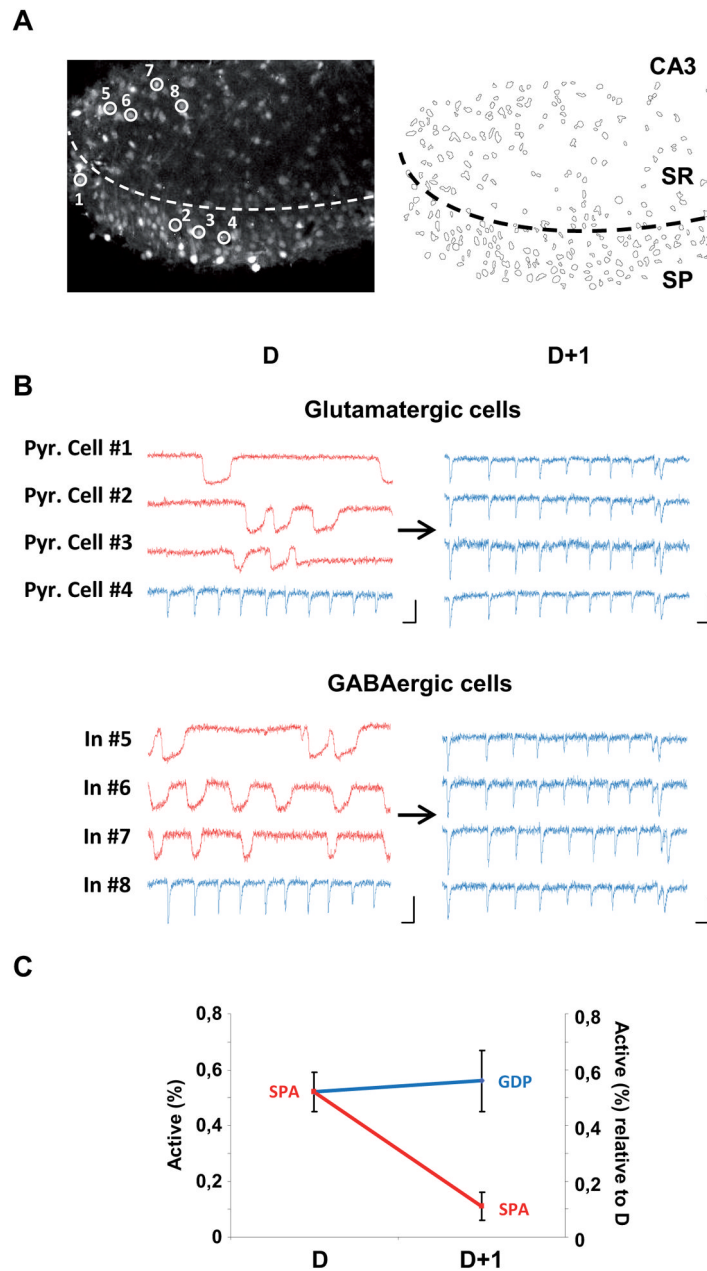


Figure 2. SPA-cells develop into GDP-cells as the hippocampal network matures

A. Two-photon calcium fluorescence image (left) and contour map of the cells imaged (right) in the CA3 region of an organotypic hippocampal slice prepared from a P4 mouse. Abbreviation: SR, *Stratum Radiatum* and SP, *Stratum Pyramidale*. B. Calcium fluorescence traces as a function of time of four pyramidal cells (Pyr. Cell #1–4) and four interneurons (In #5–8) marked in (A) and monitored after 2 days in culture (Day D) and one day later (D+1). x axis: 10 sec; y axis: 20% DF/F. Note that Pyr. Cells # 1–3 and Ins # 5–7 first produce calcium plateaus characteristic of SPAs at D and display synchronous fast calcium transients associated with GDPs at D+1. C. Diagram indicating: (1) at D: the fraction of SPA-cells relative to all active cells (y-axis on the left); (2) at D+1: the fraction of SPA- and GDP-cells relative to the number of SPA-cells at D (y-axis on the right) (n=4 slices, 520 neurons). Note

that the proportion of SPA-cells at D that become involved in GDPs the next day is greater than that still producing SPAs at D+1 ($56 \pm 5\%$ vs. $11 \pm 10\%$).

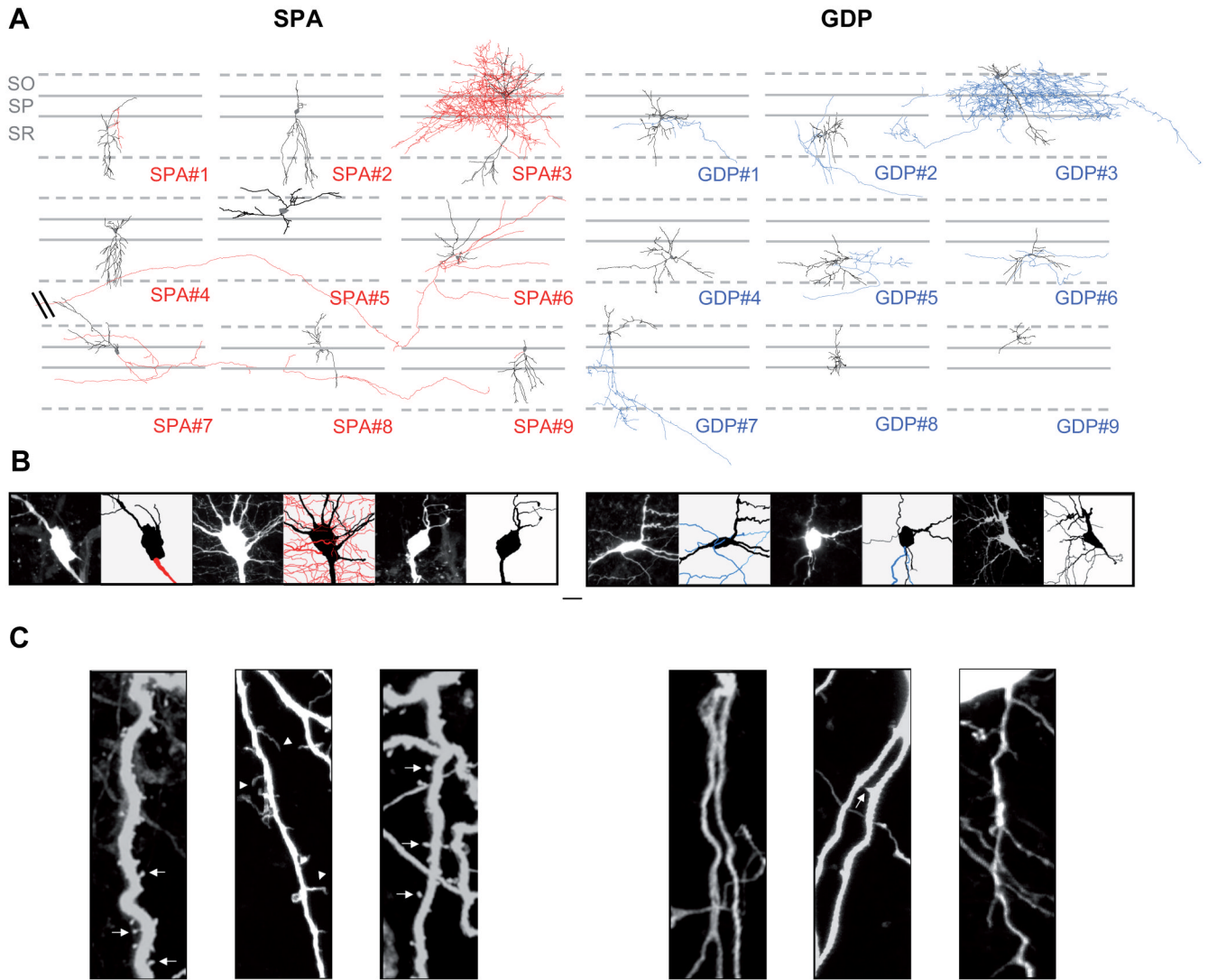


Figure 3. SPA- and GDP-interneurons are morphologically diverse with SPA-interneurons displaying larger somata and a higher density of membrane protrusions

NeuroLucida reconstructions of eighteen Neurobiotin-filled neurons, nine SPA-interneurons (left panels) and nine GDP-interneurons (right panels) from P4 GAD67-KI-GFP mice. Both groups are morphologically diverse (dendrites and soma in black, axons in red and blue for SPA- and GDP-interneurons respectively); scale bar: 50 μ m. B. Confocal fluorescence images and the corresponding neuroLucida reconstructions of the three SPA- (left insets) and three GDP-interneurons (right insets) illustrated in (A.) at a high magnification centered on the soma. Note that the soma of SPA-interneurons is larger than that of GDP-interneurons. scale bar: 50 μ m. C. Confocal fluorescence images of a fragment of second order dendritic tree for three SPA- (left panels) and GDP-interneurons (right panels) illustrated in (A.) scale bar: 5 μ m. Note that the dendrites of SPA-interneurons are covered with numerous protrusions of various shapes i.e. round and small (white arrow) or elongated (white arrowhead).

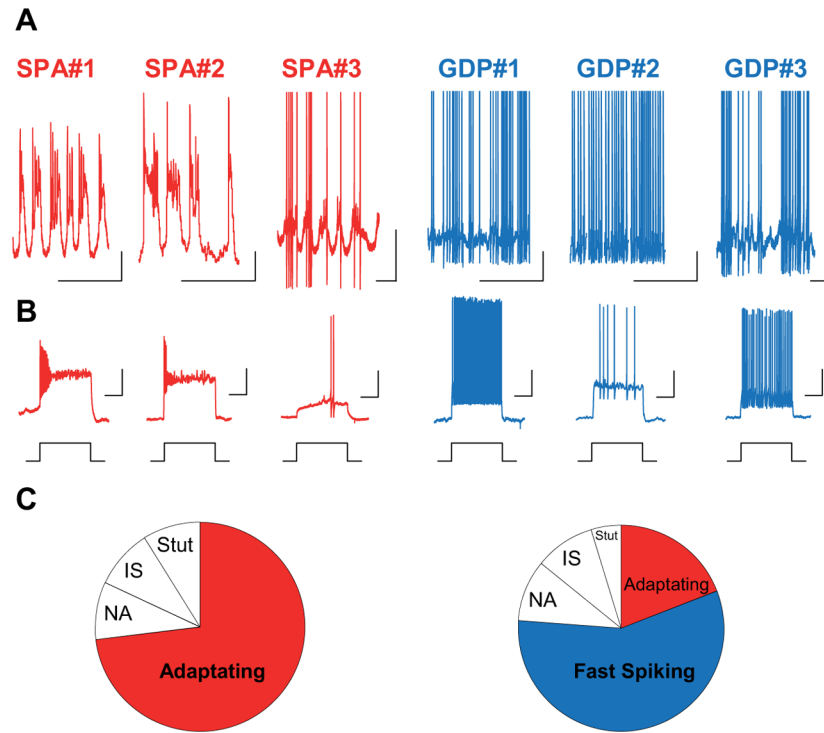


Figure 4. Different SPA-interneurons display similar intrinsic electrophysiological properties while firing diversity only emerges in GDP-interneurons

A. Electrophysiological recordings in current clamp mode, at resting membrane potential ($I=0$ pA), in the presence of blockers of synaptic transmission ($10\mu\text{M}$ bicuculline, $10\mu\text{M}$ NBQX, $40\mu\text{M}$ APV) from the three SPA-interneurons (SPA#1–3) and the three GDP-interneurons (GDP#1–3) illustrated in (Fig. 3A) from P4 GAD67-KI-GFP mice; x axis: 1 sec and y axis: 20 mV. B. Firing patterns in response to a depolarizing current step (+40 pA); x axis: 5 sec and y axis: 10 mV. Note that at the same developmental stage (P4) a basket-like SPA-interneuron (SPA#3, Fig. 3A) presents a strongly delayed and adapting firing pattern while a basket-like GDP-interneuron (GDP#3, Fig. 3A) displays a fast spiking pattern. C. Diagram representing the distribution of different firing patterns recorded in SPA-interneurons (n=11). Abbreviation: NA: Non Adaptating; IS: Irregular Spiking and Stut: Stuttering. Note that SPA-interneurons display similar intrinsic electrophysiological properties with an adapting firing pattern and recurrent membrane potential oscillations at resting membrane potential; GDP-interneurons display a diversity of firing patterns.

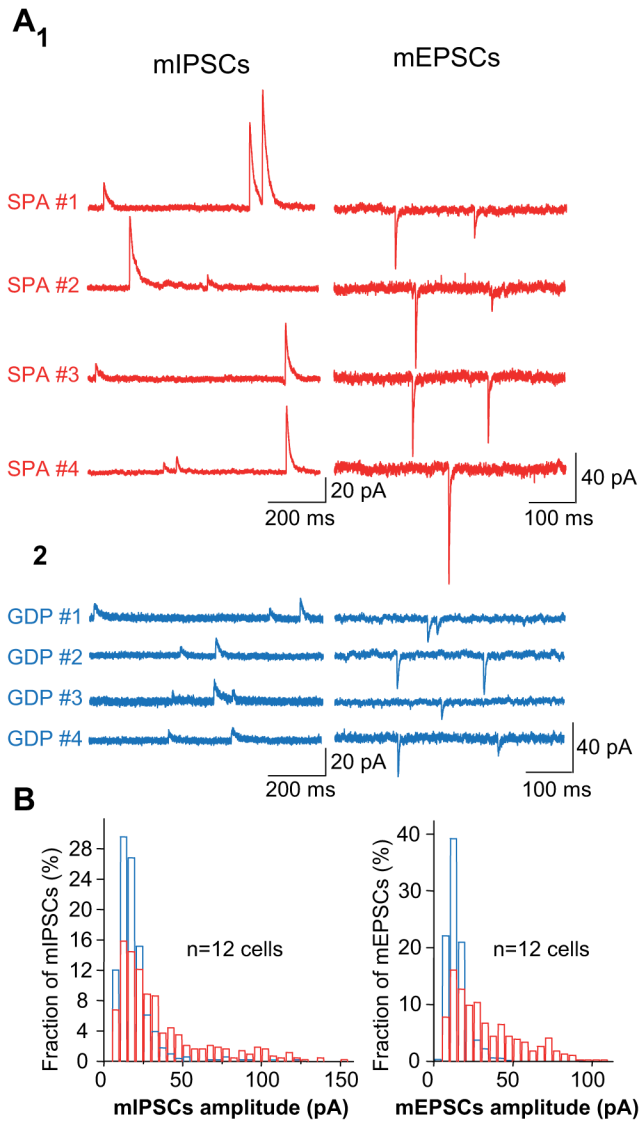


Figure 5. Large amplitude miniature postsynaptic currents are only recorded in SPA-cells
 A1. Miniature GABAA-R-mediated postsynaptic currents (mIPSCs) recorded at + 10mV and AMPA /KA-R –mediated postsynaptic currents (mEPSCs) recorded at – 60 mV in the CA3 hippocampal region of P4 GAD67-KI-GFP mice in four SPA-interneurons. A2. Same as (A1.) but in four GDP-interneurons. Note the occurrence of high amplitude mIPSC and mEPSCs only in SPA-interneurons. B. Histograms plotting the pooled distribution of mIPSCs and mEPSCs amplitudes of SPA- (red) and GDP-(blue) interneurons. Note the strong right skew of both mIPSCs and mEPSCs distributions for SPA-interneurons, indicating a large variety of event amplitudes with a significant occurrence of larger events.

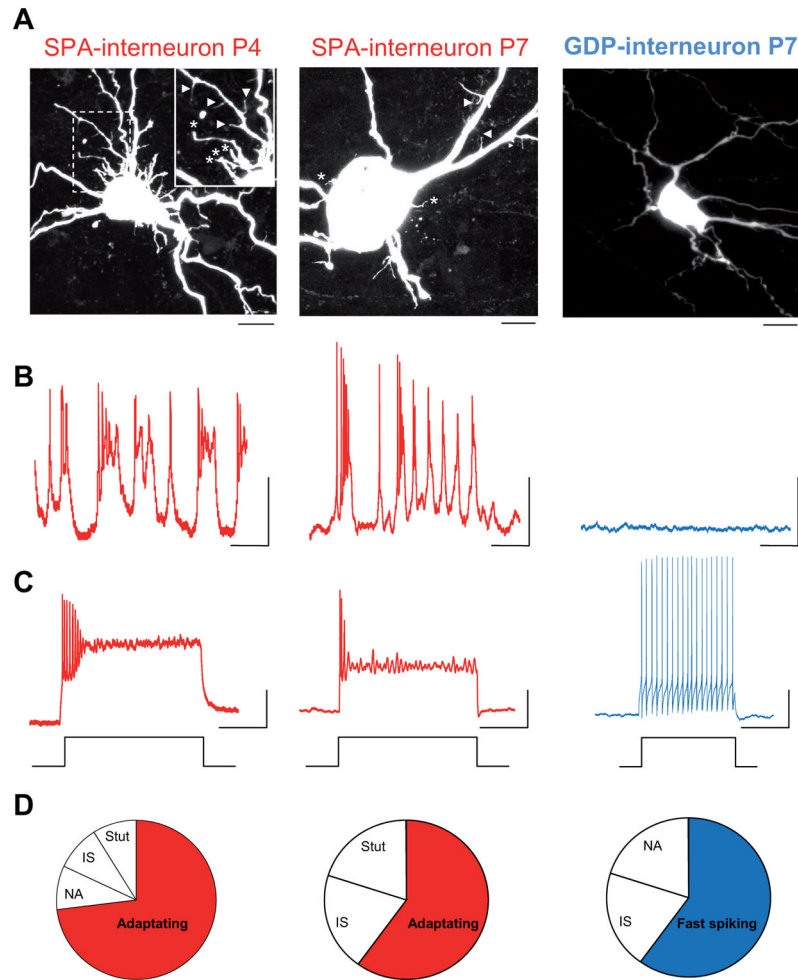


Figure 6. Morpho-physiological specificities of SPA-interneurons are age-independent

A. Confocal images of three neurobiotin-filled CA3 interneurons targeted at P4 and P7 in GAD67-KI-GFP mice: SPA-interneuron at P4 (left, inset is a higher magnification of the area indicated by the dashed rectangle), SPA-interneuron at P7 (middle) and GDP-interneuron at P7 (left). Scale bar: 10 μ m. Note the presence, at both ages, of somatic (stars) and dendritic (arrowheads) protrusions on SPA-interneurons whereas the GDP-interneuron is free of protrusions and presents a smaller cell body than SPA-interneurons. Note also the global increase in cell body size between P4 and P7. B. Electrophysiological recordings in current clamp mode, at resting membrane potential ($I=0$ pA) in the presence of blockers of synaptic transmission (10 μ M bicuculline, 10 μ M NBQX, 40 μ M APV) for the three interneurons illustrated in (A), x axis: 2 sec and y axis: 20 mV. C. Firing patterns in response to a depolarizing current step (+40 pA); x axis: 1 sec and y axis: 20 mV. D. Diagram representing the distribution of different firing patterns recorded in the three interneurons illustrated in (A) (n=11; n=5 and n=5, respectively) and showing that the adapting pattern is the most represented one in the SPA-interneuron population. Abbreviations: NA, Non Adapting; IS, Irregular Spiking and Stut: Stuttering. Note that in addition to membrane protrusions (A) both SPA-interneurons display similar intrinsic electrophysiological characteristics i.e. adapting firing patterns and recurrent membrane potential oscillations, even at late postnatal stages (P7) where only few SPA-interneurons can be found.

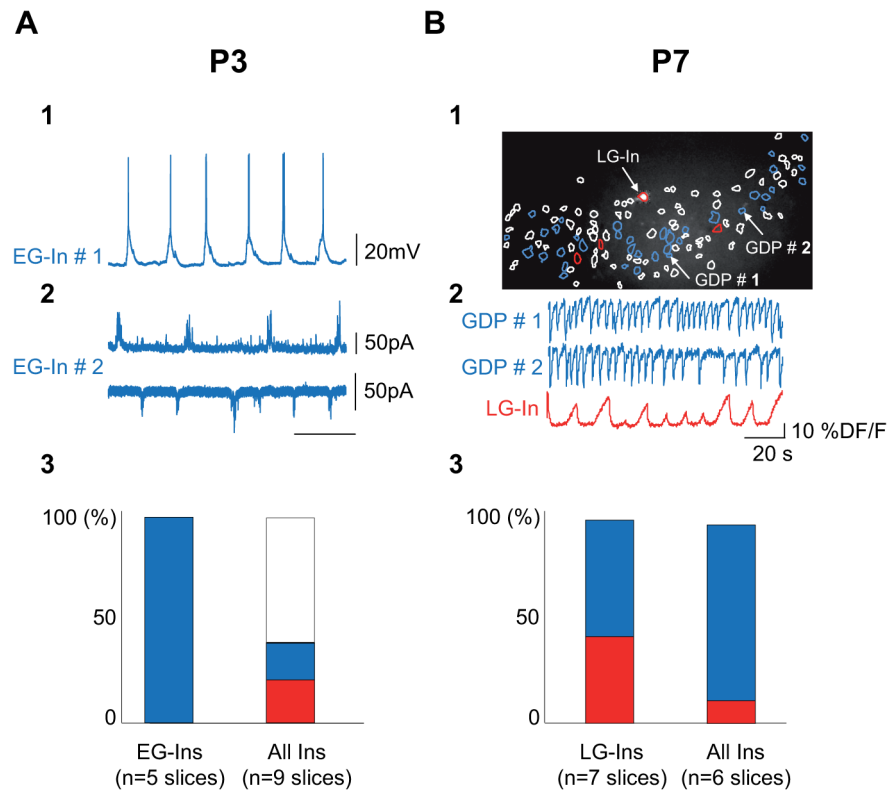


Figure 7. Interneuron involvement in SPAs or GDPs depends on birth date

A.1 Current clamp recording at resting membrane potential (0pA) of an Early-Generated Interneuron (EG-In) of the CA3 region of a P3 Mash1CreERTM;RCE:LoxP mouse treated with tamoxifen at E11.5 (see Methods). Note the presence of GDPs. A.2 Same as (A.1) but in voltage clamp mode recorded at +10mV (upper trace) and at -60 mV (bottom trace) in another EG-In. Again, note the presence of characteristic GABAergic (upper trace) and glutamatergic (bottom trace) bursts of postsynaptic currents associated with GDPs. A.3 Bar histogram indicating the fraction of SPA- (red) and GDP- interneurons (blue) at P3 (1) out of the total EG-Ins population (left) and (2) in the overall GFP positive cell population from GAD67 KI mice (right). The white part of the histogram indicates the percentage of either immature spiking or inactive interneurons. Note that all EG-Ins are already involved in GDPs at a developmental stage (P3) dominated by immature activities. B.1 GFP-positive late-generated interneuron (LG-In, red contour and white filled soma) imaged in the CA1 hippocampal region of a P7 Mash1CreERTM;RCE:LoxP mouse treated with tamoxifen at E18.5 (see Methods) and superimposed with the contour map of all imaged cells; silent cells: white contours, GDP-cells: blue contours, SPA-cells: red contours. B.2 Traces of calcium fluorescence changes as a function of time for two representative GDP-cells and for the SPA-LG-In indicated in (B.1). B.3 Bar histograms indicating the percentage of SPA- (red) and GDP- interneurons (blue) at P7 (1) out of the total population of LG-Ins from Mash1CreERTM;RCE:LoxP mice treated with tamoxifen at E18.5 (left) and (2) out the total population of GAD-GFP positive cells from GAD67 KI mice (right). Note that a large fraction of LG-Ins are still involved in SPA at a development stage (P7) dominated by GDPs.

Table

Comparison of the morpho-physiological properties of SPA- and GDP-interneurons.

	SPA	GDP
Electrophysiological properties		
Rm (MΩ)	511 ± 61 (<i>n</i> =11)*	779 ± 72 (<i>n</i> =6)
Cm (pF)	78 ± 8 (<i>n</i> =11)*	48 ± 5 (<i>n</i> =6)
Vrest (mV)	-48.4 ± 5 (<i>n</i> =6)*	-74.5 ± 3 (<i>n</i> =60.)
AP amplitude (mV)	52 ± 5 (<i>n</i> =11)*	95 ± 6 (<i>n</i> =6)
AP threshold (mV)	-54 ± 3 (<i>n</i> =11)	-62 ± 4 (<i>n</i> =6)
AP duration (ms)	4 ± 0.4 (<i>n</i> =11)*	2 ± 0.1 (<i>n</i> =6)
Postsynaptic currents		
sIPSCs		
Amplitude (pA)	35 ± 4 (<i>n</i> =5)*	29 ± 9 (<i>n</i> =5)
Frequency (Hz)	1.9 ± 0.4 (<i>n</i> =5)	2.6 ± 0.8 (<i>n</i> =5)
Rise (ms)	1.4 ± 0.2 (<i>n</i> =5)*	3.2 ± 1.2 (<i>n</i> =5)
Decay (ms)	10 ± 2 (<i>n</i> =5)*	24 ± 5 (<i>n</i> =5)
mIPSCs		
Amplitude (pA)	33 ± 4 (<i>n</i> =5)*	21 ± 6 (<i>n</i> =5)
Frequency (Hz)	0.6 ± 0.1 (<i>n</i> =6)	0.7 ± 0.5 (<i>n</i> =6)
Rise (ms)	1.4 ± 0.2 (<i>n</i> =6)	2.5 ± 1 (<i>n</i> =6)
Decay (ms)	10 ± 1.5 (<i>n</i> =6)	16 ± 4 (<i>n</i> =6)
sEPSCs		
Amplitude (pA)	23 ± 5 (<i>n</i> =5)	29 ± 7 (<i>n</i> =5)
Frequency (Hz)	1.6 ± 0.4 (<i>n</i> =5)	4 ± 2 (<i>n</i> =5)
Rise (ms)	0.8 ± 0.2 (<i>n</i> =5)	1.6 ± 0.3 (<i>n</i> =5)
Decay (ms)	3.5 ± 1 (<i>n</i> =5)	9.2 ± 3 (<i>n</i> =5)
mEPSCs		
Amplitude (pA)	30 ± 6 (<i>n</i> =6)*	16 ± 1.2 (<i>n</i> =5)
Frequency (Hz)	0.5 ± 0.1 (<i>n</i> =6)	0.4 ± 0.14 (<i>n</i> =5)
Rise (ms)	0.6 ± 0.1 (<i>n</i> =6)	1.8 ± 0.5 (<i>n</i> =5)
Decay (ms)	3 ± 0.7 (<i>n</i> =6)*	9.4 ± 1.4 (<i>n</i> =5)
Morphology		
Cell body area (μm ²)	165 ± 21 (<i>n</i> =9)*	105 ± 10 (<i>n</i> =9)
Dendrites		
Length (μm)	1422 ± 199 (<i>n</i> =9)	1206 ± 154 (<i>n</i> =9)
Surface (μm ²)	41667 ± 7163 (<i>n</i> =9)	34602 ± 7783 (<i>n</i> =9)
Nodes	21.4 ± 3 (<i>n</i> =9)	22.9 ± 4 (<i>n</i> =9)
Protrusions (# / μm)	0.25 ± 0.05 (<i>n</i> =22)*	0.14 ± 0.05 (<i>n</i> =16)
Axon		
Length	6909 ± 4863 (<i>n</i> =5)	5242 ± 3464 (<i>n</i> =6)

	SPA	GDP
Surface	403776 ± 226349 (<i>n</i> =5)	182316 ± 72865 (<i>n</i> =6)
Nodes	148 ± 135 (<i>n</i> =5)	145 ± 115 (<i>n</i> =6)

Abbreviation: Rm, Membrane Resistance; Cm, Membrane Capacitance; Vrest, Resting Membrane Potential; AP: Action Potential.

*
p<0.05 compared with GDP-cells.

*
p<0.05